

Controlling simulated outbreaks of new SARS-CoV-2 variants

Annemarie Grass², Kory D. Johnson¹, Daniel Toneian², Mathias Beiglböck², Jitka Polechová²

1 Institute of Statistics and Mathematical Methods in Economics, TU Wien, Vienna, Austria

2 Department of Mathematics, University of Vienna, Vienna, Austria

 These authors contributed equally to this work.

* kory.johnson@tuwien.ac.at

Abstract

In light of the continuing emergence of new SARS-CoV-2 variants and vaccines, we create a simulation framework for exploring possible infection trajectories under various scenarios. The situations of primary interest involve the interaction between three components: vaccination campaigns, non-pharmaceutical interventions (NPIs), and the emergence of new SARS-CoV-2 variants. New infections are generated according to a hierarchical model in which people have a random, individual infectiousness. The model thus includes super-spreading observed in the COVID-19 pandemic. Our simulation functions as a dynamic compartment model in which an individual's history of infection, vaccination, and possible reinfection all play a role in their resistance to further infections. We present a risk measure for each SARS-CoV-2 variant, ρ^V , that accounts for the amount of resistance within a population and show how this risk changes as the vaccination rate increases. Different control strategies are implemented which aim to both suppress COVID-19 outbreaks when they occur as well as relax restrictions when possible. We find that a controller that responds to the effective reproduction number in addition to case numbers is more efficient and effective in controlling new waves than monitoring case numbers alone. This is of interest as the majority of the public

discussion and well-known statistics deal primarily with case numbers.

Keywords: COVID-19, epidemic control, containment, mitigation, effective reproduction number, cross-infection, vaccination, VOC, compartment model, overdispersion, superspreading.

Author summary

The COVID-19 pandemic is constantly evolving due to the emergence of new viral variants and the discovery and distribution of multiple vaccines. Individuals are partially resistant to future infections based on both the vaccine they received as well as any previous infection, if applicable. In this setting, governments are assigned a difficult task: prevent future waves of infections from overwhelming the health care system but do not over-regulate citizens' lives.

We created a model and computer simulation that captures the complexities of the spread of the COVID-19 pandemic within a community. The model includes a risk measure for each viral variant that accounts for the amount of resistance within a population. Our model allows users to simulate interventions to reduce viral spread, e.g., social distancing requirements. We then ask: what statistics should a government consider when determining to increase or decrease restrictions? We find that responding to the effective reproduction number in addition to case numbers is significantly more effective and efficient than responding to case numbers alone. Lastly, our results highlight that the slower response arising from reacting the number of hospitalization is considerably less efficient in containing outbreaks.

Introduction

The continued waves of the COVID-19 pandemic present unique challenges to regulatory bodies and governments. At issue is the balance between restricting behavior in order to reduce the spread of SARS-CoV-2 and the desire to return to a normal state-of-affairs. On one hand, many countries provide a deluge of statistics to measure the severity of COVID-19, sometimes even on the county level. These statistics then

inform complex decisions on how many restrictions to enforce. On the other hand, some countries lack sufficient testing to accurately track the spread of COVID-19. Our guiding question is, what statistics should be considered when determining if mitigation measures should be increased or decreased? Of concern is the oft-repeated scenario in which a new variant emerges which spreads more rapidly either due to increased infectiousness or vaccine escape.

To this end we create a compartment model that has compartments for each vaccinated, infected, and recovered group (for each variant), and add dynamic interactions between these groups. For example, someone could have been infected with the original SARS-CoV-2 variant, then receive a vaccine, then perhaps later become infected with a new SARS-CoV-2 variant. The resistance to further infection conferred by such a history is distinct from those who have, for example, only been vaccinated. These factors influence the effective reproduction number, or the expected number of new infections caused by a currently infected individual. We can then simulate infections using this model in order to answer questions about case dynamics when a new SARS-CoV-2 variant is introduced.

We also add a controller to our simulations, which can both observe and intervene in the compartment model. The controller is thought of as a governing agent which is responsible for both keeping COVID-19 outbreaks at manageable levels and not imposing unnecessary restrictions, i.e., for keeping outbreaks under “control.” In order to mimic a real-life entity such as a government, the controller must be constrained in various ways. First, the controller does not observe latent variables such as infectiousness, only raw data such as number of new infections (for each variant). Second, these statistics are observed with a lag, i.e., there is a delay between when infections occur and when they are observed. Third, the controller uses non-pharmaceutical interventions (NPIs) such as mask wearing, testing and tracing, and gathering restrictions (soft lockdowns) – which mitigate the effective reproductive number of SARS-CoV-2. Lastly, these interventions cannot change continuously: there is a mandatory temporal gap after an intervention before the controller can intervene again.

Under these constraints, we are able to explore what statistics the controller needs to respond to in order to effectively suppress new outbreaks. Note that we are not

advocating a particular intervention or comparing their efficiency [1, 2]. Instead, we are considering what information could best inform timely decisions on modifying NPIs. Furthermore, we note that the success of the controller we implement is often not mirrored in reality as few if any governments willingly act as rapidly as stipulated. For example, the World Health Organization issues guidelines for COVID-19 risk [3, 4], but immediate action is often not taken when a country crosses one of the thresholds they provide. This is exacerbated by the lag between infection and observation (the “delay” parameter): governments which either fail to collect adequate data or do not make decisions using a forecast will make decisions with greater delay.

Other recent works have considered similar topics. [5] posits economic models that convert the effect of NPIs on both public health and the economy into a single cost measure. Using infection forecasts from SEIR models, they then optimize decision thresholds which depend solely on the number of cases. The infection models used do not contain any diversity in SARS-CoV-2 variants or vaccines. On a different level of analysis, [6] proposes a procedure for expert elicitation in order to synthesize the results from multiple modeling groups to improve intervention planning.

We begin by presenting a detailed description of our model. This is broken up into subsections which describe the compartment model with different vaccines and variants, the controllers we consider, and how the simulation is initialized to mimic a real outbreak. In the Results section, we compare the modelled dynamics of the SARS-CoV-2 variants, as well as the controllers’ effectiveness in containing both current and hypothesized variants. Last, we discuss broader implications of our research and further questions which could be explored within the framework.

Methods

New infections are assumed to be generated according to the momentum model of Johnson *et al.* [7], which builds upon Cori *et al.* [8]. In the simplest case, new infections I_t are the result of previous infections I_1, \dots, I_{t-1} via the following recursion:

$$I_t \sim \text{Poisson} \left(\mathcal{R}_{e,t} \sum_{m=1}^{\nu} I_{t-m} w_m \right), \quad (1)$$

where $\mathcal{R}_{e,t}$ is the time-varying effective reproduction number at time t , $\mathbf{w} = (w_1, \dots, w_\nu)$ is the generation interval, and ν is the maximum number of days for which someone is assumed to be infectious. If J_m denotes the number of people infected by a specific person on the m -th day after this person got infected, then we have for $m \in \mathbb{N}$

$$w_m = \frac{\mathbb{E}[J_m]}{\sum_{l=1}^{\infty} \mathbb{E}[J_l]}.$$

We assume that a newly infected individual does not cause secondary cases on the same day, corresponding to $w_0 = 0$, and that infections do not occur after day ν . The generation interval can be interpreted as the infectiousness profile of infected persons. We set \mathbf{w} to be a discretized gamma distribution with $\nu = 13$, mean 4.46, and standard deviation 2.63. These are values specific to Austria [9], and are similar to values determined elsewhere [10, 11].

The recursion in Equation (1) assumes that all people have the same infectiousness on day t : $\mathcal{R}_{e,t}$. We follow [7] and remove this assumption by explicitly drawing an infectiousness parameter for each infected person from a fixed Gamma distribution with dispersion parameter $k < 1$. This generalization allows for superspreading: the phenomenon of extreme heterogeneity in infectiousness. We set $k = 0.1$, which corresponds to a setting in which 10% of infected individuals cause 80% of new infections [12]. This is an integral component of the difficulty of controlling COVID-19 outbreaks. Individual infectiousness can be aggregated over the infected, resulting in the following process of new infections:

$$I_t \sim \text{Poisson} \left(\sum_{m=1}^{\nu} \theta_{t-m} w_m \right) \quad \text{where} \quad (2)$$

$$\theta_s \sim \text{Gamma}(I_s k, \text{rate} = k / \mathcal{R}_{e,t}). \quad (3)$$

We generalize this model further in order to study the effect of combinations of variants, previous infections, vaccination strategies, and NPIs – and interactions between them – on the effective reproductive number $\mathcal{R}_{e,t}$. This is done by decomposing $\mathcal{R}_{e,t}$ into many constituent parts which depend on the compartments in

our model. In order to describe this decomposition, we need notation for compartments.

Our model contains a set of compartments \mathcal{C} . Each compartment $\mathcal{C} \in \mathcal{C}$ is a group of people with a unique infection and vaccine history. The history is encoded as a superscript h : \mathcal{C}^h . The value of h contains both digits and capital letters, where digits correspond to vaccines and letters correspond to different SARS-CoV-2 variants (when possible, the first letter of the variant name). For example, a group with label $h = A1B$ contains people that were first infected with variant A (Alpha), then vaccinated with vaccine 1, then contracted variant B (Beta). For simplicity, the digit 0 is reserved for the compartment that has neither been vaccinated nor contracted SARS-CoV-2 of any form, i.e., \mathcal{C}^0 .

The only characteristics of the history that effect the model are the total set of experiences (vaccines or infections) as well as the final infection, as this determines the variant one is infectious with. Furthermore, reinfection with the same variant does not confer additional benefit. Hence we can simplify histories to those that have no repeated characters. Lastly, at times it will be easier to write equations using the set of histories, \mathcal{H} , instead of the corresponding set of compartments, \mathcal{C} . As $h \in \mathcal{H}$ is the identifier of a compartment, we will also at times call it a compartment for ease of use.

Each group \mathcal{C}^h contains the total number of people with that history, both infected (I^h) and recovered (S^h), which are subgroups with the same labels: $\mathcal{C}^h = I^h \cup S^h$. The recovered (or vaccinated) subgroup is written as S^h to emphasize that they are again susceptible to infection, though with a resistance parameter depending on h as described below. All are given subscripts t , though for consistency with the generating equations, the subscripted groups have different interpretations. \mathcal{C}_t^h and S_t^h contain *all people* on day t with history h and the subset that are recovered, respectively. I_t^h gives the number of *new* infections with history h on day t . For simplicity, individuals recover $\nu + 1$ days after being infected. We assume that when one is experiencing an infection, they cannot become newly infected (or receive a vaccine). With these simplifications, we have $|\mathcal{C}_t^h| = |S_t^h| + \sum_{m=1}^{\nu} I_{t-m}^h$. Note that notation for I_t^h has been overloaded to either be the set of people with new infections with history h or the cardinality of this set. This provides consistency with the generating Equation (2).

An important aspect of the simulation is that interaction groups are created dynamically. For example, someone in S_t^h can be infected with a SARS-CoV-2 variant

D or become vaccinated with vaccine 4. This person then moves from S_t^h to a new group with identifier hD or $h4$, respectively. The dynamic generation of groups goes hand-in-hand with a dynamic change of population characteristics which may require different mitigation strategies. Crucially, the new group hD or $h4$ can have new resistances to infection.

There is a specific $\mathcal{R}_{e,t}^{gh}$ for all compartments $h, g \in \mathcal{H}$, where group I^h is able to infect group S_t^g on day t . Clearly this is not possible for all compartments C^h , as not all compartments are infectious, e.g., $I_t^0 := 0 \forall t$. In these cases, $\mathcal{R}_{e,t}^{gh} = 0, \forall g \in \mathcal{H}$. This is done for convenience such that we do not have to specify restrictions on the label h for all equations presented in the paper. As data are often reported in terms of relative transmissibility of SARS-CoV-2 variants, each infected group I^h has a basic reproduction number relative to that of the original SARS-CoV-2 variant given by $\mathcal{R}_0^h = \lambda^h \mathcal{R}_0$. As above, this only depends on the final index of h . If h is a non-infectious compartment (its final index is a number), then $\lambda^h = 0$.

With this group-specific notation, we can define a decomposition of $\mathcal{R}_{e,t}^{hg}$ as

$$\mathcal{R}_{e,t}^{hg} = \lambda^g \mathcal{R}_0 \tilde{\gamma}^{hg} \tilde{M}_t L_t \quad (4)$$

where

- $\tilde{M}_t = (1 - M_t)$ where $M_t \in [0, 1]$ is the effectiveness of NPIs at time t (mitigation of infectiousness). $\tilde{M}_t = 1$ corresponds to no mitigation (full infectiousness), whereas $\tilde{M}_t = 0$ reduces new infections to 0.
- L_t is a seasonality factor at time t .
- $\tilde{\gamma}^{hg}$ is the susceptibility of group h to infection from group g . We consider $\tilde{\gamma}^{hg} = (1 - \gamma^{hg})$ where $\gamma^{hg} \in [0, 1]$ is the *resistance* of group S^h to being infected by group I^g . The value of γ^{hg} depends both on the infection carried by I^g as well as the unique history h .

Similar to other human coronaviruses and influenza viruses [13, 14], it is widely believed that SARS-CoV-2 follows a seasonal transmission pattern in temperate regions with transmissions peaking during the winter. Possible explanations include different

viral longevity due to humidity and air temperature [15,16], reduced host airway immune response in dry winter months [14,17], and increased indoor interactions during colder months. We model seasonality, L_t , as in [18] via a cosine transform:

$$L_t = 1 + \frac{\epsilon}{2} \left(\cos \left(2\pi \frac{t - t_{peak}}{365.25} \right) - 1 \right), \quad (5)$$

where ϵ is the amplitude size and t_{peak} is the date when the transmission rate peaks. Following [19], we assume that the seasonal reduction in transmission is 40% ($\epsilon = 0.4$); the lowest transmission rate is set to July 1, while the highest transmission rate occurs on $t_{peak} =$ January 1. This is in line with the estimates for the general seasonality of other coronaviruses in temperate climates [13].

The resistance parameters γ^{hg} evolve according to two simple rules. First, if a person with history h is given a vaccine (e.g. 1), resulting in history $g = h1$, they have variant-specific resistances equal to the maximum from those provided by h and 1. For example, history h may provide resistance .9 for infection from variant D and .98 for variant A . Vaccine 1, on the other hand, provides resistance .95 for both. The resulting resistance for g is thus .95 for D and .98 for A . All resistance parameters are given in Table 1.

Second, if a person with history h is infected by a variant V , resulting in history $g = hV$, we consider both the resistances of h and those conferred by V . For this new history g , the resistance to an infection with a different SARS-CoV-2 variant V' is given by

$$\gamma^{gV'} = 1 - (1 - \gamma^{VV'})(1 - \gamma^{hV'}), \quad \text{equivalently} \quad (6)$$

$$\tilde{\gamma}^{gV'} = \tilde{\gamma}^{VV'} \tilde{\gamma}^{hV'}. \quad (7)$$

We note here that interactions between groups are only considered in terms of resistances, not in terms of infectiousness; a vaccinated individual that nevertheless gets infected with variant V is considered equally infectious as an unvaccinated individual infected with variant V . This is a simplification – in reality, the viral load in infected, vaccinated individuals appears to decline faster (and is hence lower on average) [20]. In

addition, for the same nasopharyngeal viral load (C_{ts}), the probability of detecting an infectious virus using cell culture is also slightly lower [21]. While the model can be extended to include some estimate of lower infectiousness for an infected, vaccinated group, we chose not to do so at present; we do not have a quantitative estimate of how reduced infectiousness translates into reduction in transmission probability in real-life settings, particularly as vaccinated individuals may behave differently. Secondly, we ignore the effect of vaccine waning, which acts in the opposite direction.

Specifying the infections created by I^h is notationally far more complex than in equations (2) and (3). The issue is that I^h is not solely responsible for creating new infections with this same history at time t : I_t^h . This problem arises even in the most simplistic multi-variant-vaccine setting. Given compartments \mathcal{C}^0 , \mathcal{C}^1 , \mathcal{C}^A , and \mathcal{C}^{1A} , consider the effects of infection and vaccination. New cases I_t^A are produced by both I^A and I^{1A} when they infect members of S^0 , while new cases I^{1A} are produced when either I^A or I^{1A} infect members of S^1 , or S^{1A} . Vaccine 1 is administered to a random member of either S^0 or S^A , and adds members to either S^1 or S^{1A} , respectively.

Given these complexities, we provide simple equations that only show the new infections of a specific history. While it is possible to provide equations for the total new cases for a variant V , this would complicate our expressions and amounts to summing over many different compartments that are distinct in our model. Later, Equation (13) provides variant-specific equations in some settings as a way to compare infectiousness of variants in a population.

For consistency of notation, our generating equations describe the number of new infections of a variant V *within a compartment* \mathcal{C}^g . To do so, consider all compartments which are infectious with V : $\{h \in \mathcal{H} \text{ s.t. } h = \bar{h}V, \text{ for some history } \bar{h}\}$. Each \mathcal{C}^h creates new infections in S^g according to equations (2) and (3). We then sum over these groups.

$$I_t^{gV} \sim \text{Poisson} \left(\tilde{M}_t L_t N^{-1} \sum_{\substack{h \in \mathcal{C} \\ \text{s.t. } h = \bar{h}V}} \tilde{\gamma}^{gh} |S_t^g| \sum_{m=1}^{\nu} \theta_{t-m}^h w_m \right) \quad \text{where} \quad (8)$$

$$\theta_s^h \sim \text{Gamma}(I_s^h k, \text{rate} = k(\lambda^h \mathcal{R}_0)^{-1}) \quad (9)$$

and N is the total population size, $N = \sum_{\mathcal{C} \in \mathcal{C}} |\mathcal{C}|$.

Observe that θ_s^h depends on $\mathcal{R}_0^h = \lambda^h \mathcal{R}_0$ instead of $\mathcal{R}_{e,t}^{hg}$. This is because θ_s^h gives the “native infectiousness” of $-$ and is solely a property of $- I_s^h$, separate from the interaction between I^h and S_t^h in the environment experienced at time t . Similarly, the second sum of the Poisson argument, $\sum_{m=1}^{\nu} \theta_{t-m}^h w_m$, does not depend on g because it represents the total infectiousness of \mathcal{C}_t^h . New infections, however, depend on other groups h and the environment through the remaining parameters in Equation (8). If we ignore resistance $\tilde{\gamma}^{gh}$ and the proportion of infected people in the population is small, we have $N^{-1} \sum_{h \in \mathcal{C}} \tilde{\gamma}^{gh} |S_t^h| \approx 1$. In this case, Equation (8) reproduces (2) in the original setting of the momentum model for a single variant [7].

Controllers

We assume a controller is interested in constraining the observed process of new infections, $I_t = \sum_{h \in \mathcal{H}} I_t^h$, and can manipulate \tilde{M}_t . Changes in non-pharmaceutical interventions (NPIs) are concretely implemented by setting $\tilde{M}_{t+1} = \delta \tilde{M}_t$ in Equation (8). Thus, increase in NPIs such as mask mandates have the effect of a multiplicative decrease in transmissibility. We have explicitly assumed a certain compound *effect* of NPIs rather than specifying them. Our goal is not to prescribe which combination of NPIs to use, but to demonstrate differences in efficiency of containment strategies that result from using different statistics to guide the decision on the timing of the NPIs.

We consider two types of controllers which react to different statistics computed from case data. Both increase and decrease mitigation, \tilde{M} , by some proportion $\delta \in [0, 1]$ whenever they intervene. The first controller changes the effect of NPIs when daily cases pass pre-specified boundaries and is termed a “reactive” controller. This is a controller which increases NPIs when reported daily cases are over some high threshold (e.g. 150 per 100,000 over the last 14 days) and decreases NPIs for case numbers below a low threshold (e.g. 25 per 100,000 over the last 14 days) so long as case numbers are not increasing. A second type of controller, termed “proactive”, also utilizes an estimate of the effective reproduction number.

Let $\bar{\mathcal{R}}_{e,t}$ be the effective reproduction number given aggregate statistics which ignore the type of infection. It can be computed by equating the argument in Equation (1) with the expected sum of infections for all groups from Equation (8):

$$\bar{\mathcal{R}}_{e,t} = W^{-1} \sum_{h \in \mathcal{H}} \left(\tilde{M}_t L_t N^{-1} \sum_{g \in \mathcal{H}} \tilde{\gamma}^{hg} |S_t^h| \sum_{m=1}^{\nu} \theta_{t-m}^h w_m \right) \text{ where} \quad (10)$$

$$W = \sum_{h \in \mathcal{H}} \sum_{m=1}^{\nu} I_{t-m}^h w_m. \quad (11)$$

While Equation (10) provides a useful summary as an average effect implied by our model which accounts for variant heterogeneity, population diversity, and superspreading, it is not feasible for a controller to compute as it depends on the unknown parameters θ^h . A feasible estimator does not consider θ_t^h to be known, using instead its expectation given λ^h and \mathcal{R}_0 :

$$\hat{\mathcal{R}}_{e,t} = W^{-1} \sum_{g \in \mathcal{H}} \left(\tilde{M}_t L_t N^{-1} \sum_{h \in \mathcal{H}} \tilde{\gamma}^{hg} |S_t^h| \sum_{m=1}^{\nu} \lambda^h \mathcal{R}_0 I_{t-m}^h w_m \right). \quad (12)$$

We note that the statistic above is not meant to be an ideal estimate of the effective reproduction number $\mathcal{R}_{e,t}$, but instead functions as a computationally efficient way to track the spread of infections in a way that is consistent with our simulation framework. While quantities such as $|S_t^h|$ are not known in practice, they can be estimated per variant and vaccine. In fact, this is done when initializing our model and is described extensively later.

Given I_t and the estimated reproduction number, $\hat{\mathcal{R}}_{e,t}$, a “proactive” controller changes mitigation measures based on $\hat{\mathcal{R}}_{e,t}$ and case numbers. Behavior is the same as for the reactive controller, except that there is also an upper bound specified for $\hat{\mathcal{R}}_{e,t}$: when effective reproduction number increases beyond this upper bound, restrictions are increased. Reducing restrictions requires $\hat{\mathcal{R}}_{e,t} < 1$ in addition to low case numbers.

Vaccines and Variants

Our model includes two types of vaccines and six SARS-CoV-2 variants. Vaccine types are summarized in two groups: i) mRNA vaccines which include both Pfizer-BioNTech’s Comirnaty (BNT162b2) and Moderna’s Spikevax (mRNA-1273); and ii) vector vaccines which include AstraZeneca’s Vaxzevria/Covishield (AZD1222) and Janssen’s COVID-19

vaccine (JNJ-78436735).

We consider six variants: the original wild-type (WT), Alpha (B.1.1.7), Beta (B.1.351), Gamma (P.1), Delta (B.1.617.2) variants, and a hypothetical variant Omega. In general, their relative advantage and effective reproduction number depend on the composition of the population. The first row of table 1 shows the assumed relative advantage of variant V over the wild-type, $\lambda^V = \mathcal{R}_0^V / \mathcal{R}_0^{WT}$, in a naïve population. The values are computed from recent estimates of $\mathcal{R}_e^{V_i} / \mathcal{R}_e^{V_j}$ using GISAID sequences across different countries which are then aggregated to produce a summary estimate for each variant [22]. In general, this value is thus confounded with acquired advantage due to immunity escape, although the departure appears small within the time frame of the study (until June 3, 2021). The values are consistent with estimates of λ^V assuming substantial immune escape [23, 24] and are on the lower boundary generally accepted for the transmissibility advantage of Delta [25].

We assume that the basic reproduction number of the original strain \mathcal{R}_0^{WT} is approximately 3.5. There is a wide range of estimates of \mathcal{R}_0^{WT} , ranging from about 2 to 6.5 [26, 27]. As \mathcal{R}_0^{WT} depends on interaction networks in a society and will therefore plausibly differ between countries and regions, we use an estimate of \mathcal{R}_0^{WT} from the early Austrian case data [28, p.13], corrected for the assumed seasonality of 40%.

Table 1 summarizes both the assumed effectiveness of the vaccines against infection with SARS-CoV-2 variants as well as the estimates of resistance conferred by previous infection. We use estimates from the recent analysis by [29] (United Kingdom) concerning infections (with RT-qPCR's $C_t < 30$) by the Alpha and Delta variants. While [29] assesses subjects PCR-tested in weekly intervals, it is limited to people younger than 65 years old. We thus extend the lower bound of effectiveness following [30], which also gives estimates for effectiveness of both mRNA vaccines against (symptomatic) infections with Gamma/Beta variants (in Ontario, Canada). We also use estimates from Brazil [31] for the reduction of transmission of the Gamma variant following full vaccination with vector vaccines, and from Qatar [32] and South Africa [33] for the Beta variant. For computational simplicity, we use the resistances after a full vaccination (typically, two doses), and assign this 2 weeks after the first dose of a vector vaccine or 3 weeks for an mRNA vaccine. This is because the error arising from assigning full immunity 1-2 weeks after second dose would be larger than

neglecting slightly lower immunity between doses [29,34–36]. We assume the percentage of people who do not follow up with the second dose (when required) is sufficiently low that it can be ignored.

The reduction of probability of reinfection is based on the estimates by [29] for the WT, Alpha, and Delta variants. We assume that the probability of transmission from reinfection is reduced by 87% (84 – 90%) upon prior infection with the same variant, and it is reduced less (by 77%, (66 – 85%)) for the Delta variant when the previous infection was by a different variant (typically WT or Alpha). There is less reliable information on the reduction of re-infection for the Beta and Gamma variants. We use the model-based estimate by [24] of 70% cross-immunity (55-80%) for the Gamma variant. Based on the relative sensitivity of the variants to convalescent sera [37,38] – and in the absence of a direct estimate of reinfection protection for the Beta variant based on a random cross-infection survey – we employ the 70% cross-immunity for the Beta variant as well. The resistances are set to approximately 0.75 for cross-immunity between (typically rare) combinations where we do not have direct data, and to approximately 0.85 for reduction in reinfection by the same strain. See Table 1 for exact values.

Lastly, we ignore the effect of immunity waning after vaccine or previous infection within the period of simulation; it is clear however that for a longer time-frame, immunity waning – and effect of boosting for particular groups – would need to be considered [39,40], preferably while also including age (risk) structure.

Initializing the Simulation

Given the initial conditions, the equations given in 8 and 9 control all new infections and vaccine schedules specify new vaccinations. To initialize the simulation, we need to specify an initial collection of compartments \mathcal{C} , a vaccine schedule, and a level of NPIs. These are chosen to most accurately represent the pandemic in Austria.

Epidemiological data in Austria is gathered and provided by AGES (Agentur für Gesundheit und Ernährungssicherheit GmbH), the Austrian agency for health and food safety [41]. In addition to tracking the number of infections, hospitalizations, deaths, and tests, AGES tracks the genome sequencing of SARS-CoV-2 samples gathered in Austria to monitor the prevalence of variants of concern (VOC). The first confirmed

Table 1. Model parameters for different variants. The first row gives the assumed increase of \mathcal{R}_0 relative to wild-type (WT) based on [22]. The rest give the immunity against new infection following vaccination or previous infection. The upper row per label gives the median estimate; the lower row gives a confidence interval. The references are given in the superscript of the median value. See the text for more details.

Label	WT	Alpha	Beta	Gamma	Delta	Omega
λ^V	1 -	1.3 (1.24,1.33)	1.25 (1.2,1.3)	1.40 (1.22,1.48)	2.10 (1.76,2.17)	1.55 (1.35,1.75)
mRNA	0.94 ^[29,30] (0.85,0.96)	0.94 ^[29,30] (0.85,0.96)	0.75 ^[32] (0.7,0.8)	0.85 ^[30] (0.7,0.93)	0.84 ^[29,30] (0.7,0.86)	0.5 (0.4,0.6)
vector	0.86 ^[29] (0.65,0.93)	0.86 ^[29] (0.65,0.93)	0.1 ^[33] (0,0.55)	0.65 ^[31] (0.6,0.8)	0.7 ^[29] (0.65,0.73)	0.4 (0.3,0.5)
WT	0.87 ^[29] (0.84,0.9)	0.87 ^[29] (0.84,0.9)	0.7 ^[24] (0.55,0.8)	0.7 ^[37,38] (0.55,0.8)	0.77 ^[29] (0.66,0.85)	0.4 (0.3,0.5)
Alpha	0.87 ^[29] (0.84,0.9)	0.87 ^[29] (0.84,0.9)	0.7 ^[24] (0.55,0.8)	0.7 ^[37,38] (0.55,0.8)	0.77 ^[29] (0.66,0.85)	0.4 (0.3,0.5)
Beta	0.75 (0.65,0.85)	0.75 (0.65,0.85)	0.85 (0.8,0.9)	0.7 ^[37,38] (0.55,0.8)	0.75 (0.65,0.85)	0.4 (0.3,0.5)
Gamma	0.75 (0.65,0.85)	0.75 (0.65,0.85)	0.7 ^[24] (0.55,0.8)	0.85 (0.8,0.9)	0.75 (0.65,0.85)	0.4 (0.3,0.5)
Delta	0.75 (0.65,0.85)	0.75 (0.65,0.85)	0.7 ^[24] (0.55,0.8)	0.7 ^[37,38] (0.55,0.8)	0.85 (0.8,0.9)	0.4 (0.3,0.5)
Omega	0.75 (0.65,0.85)	0.75 (0.65,0.85)	0.7 (0.55,0.8)	0.7 (0.55,0.8)	0.75 (0.65,0.85)	0.85 (0.8,0.9)

case of the Alpha variant in Austria was on January 3, 2021. A VOC sentinel system was subsequently established with one PCR test lab per county submitting a random sample of SARS-CoV-2 specimens for complete genome sequencing.

VOC prevalence in Austria is published online and updated roughly every one to two weeks. Figure 1 provides the historical reported variant prevalences. 2021 has already seen two new variants emerge and quickly become dominant. In Austria, Alpha took approximately 15 weeks between emergence and dominance, whereas Delta took a mere 10 weeks. Both Beta and Gamma variants were observed in Austria, though neither variant made serious headway into the population.

When simulations are initialized for a given date, the relative size of recovered compartments are given using data from Figure 2. To compute the number of people who were previously infected, we must account for the detection ratio throughout the entirety of the pandemic. Based on [42] and consistent with seropositivity in Austria from mid November [43], we assume that 12% of the Austrian population had an infection with the wild-type before January 1, 2021. For 2021, we specify the detection

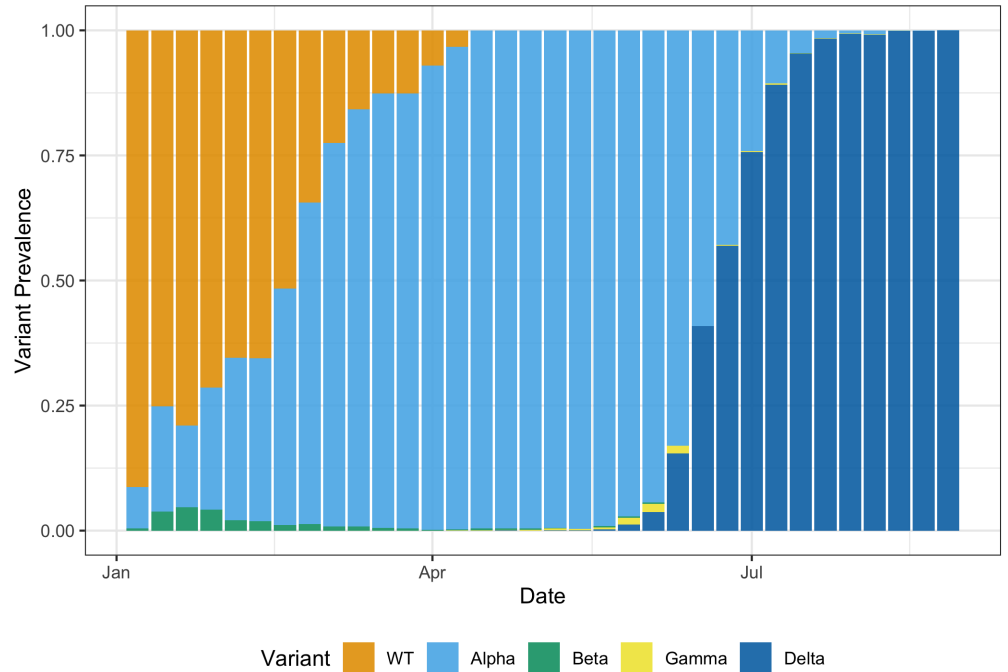


Fig 1. Reported prevalence of different SARS-CoV-2 variants in Austria in 2021 (as of August 31, 2021; data is reported approximately three weeks after samples are collected).

ratio which measures the (age-averaged) probability that an infected individual is diagnosed and appears in the official case statistics. Due to increases in the availability and use of COVID-testing in Austria, we use the following estimates for the detection ratio in 2021: $1/2,3$ for January and February, $1/2$ for March and $1/1,4$ for April and beyond. These are consistent with model-based estimates for Austria which use hospitalizations and deaths to learn about the proportion of unreported cases [28,44].

We use a vaccine schedule to match that of Austria throughout the simulation period. We use the 7-day median of administered first doses during each calendar week [45] up until August 8, 2021. When simulating beyond the window of available data, we use the latest 7-day median and administer this many doses until the expected upper bound on vaccinations is reached. Currently, this bound is 85% of the population. As of August 8, 2021, the distribution of administered vaccines was 72% Pfizer-BioNTech’s Comirnaty, 10% Moderna’s Spikevax, 15% AstraZeneca’s Vaxzevria, and 3% Janssen’s COVID-19 vaccine. Beyond August 8, the distribution of newly administered doses is 74% from Pfizer, 3% Moderna, 22% Janssen, and 1% from AstraZeneca.

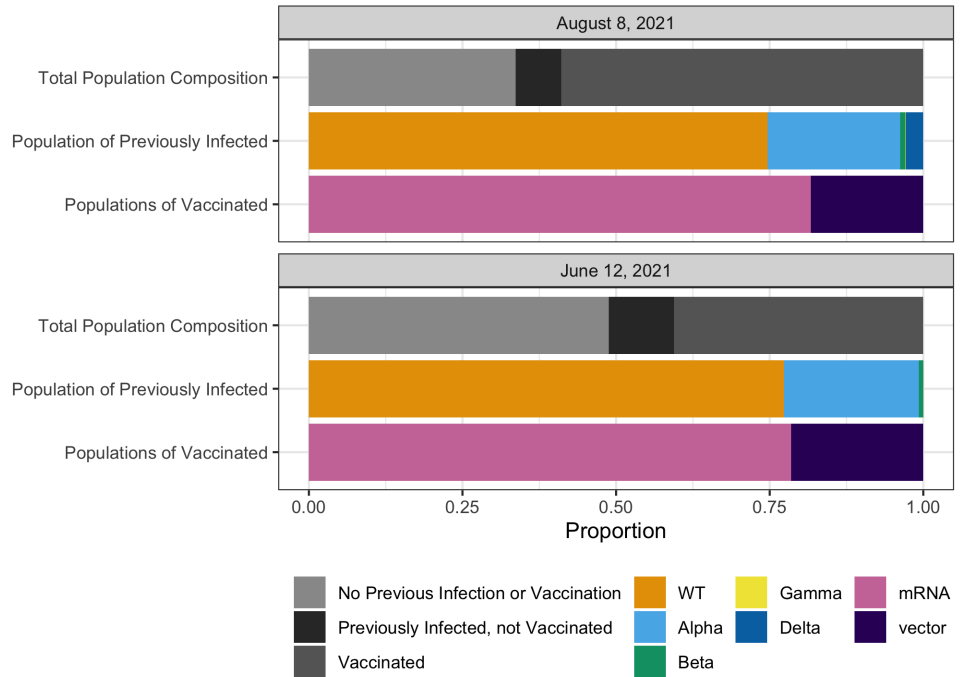


Fig 2. Estimate of the population composition in Austria on June 12 and August 8, 2021.

A final step to calibrate our model with current case numbers is to set an initial effect of NPIs. This is done by equating the implied reproduction number from the simulation, $\hat{\mathcal{R}}_{e,t}$, to the estimated \mathcal{R}_e in Austria at the time the simulation starts.

Results

This section presents simulation results for a setting constructed to be similar to that in Austria. This serves to anchor the simulation in a realistic setting, though the high-level results are applicable beyond Austria as well. To aid comparisons to other countries, data are reported as cases/100,000 inhabitants.

Comparing Variants

Ultimately, our model requires many parameters to be set which govern the resistance one variant provides to infection from others, as well as resistances conferred due to vaccines. There are three relevant dimensions in which we allow variants to differ: the basic reproduction number \mathcal{R}_0^h , immune escape after vaccination, and immune escape

after infection. It is important to view these as three separate components, and we note that increasing severity in multiple categories may over-estimate the true risks of different variants. Consistent with known estimates, we assume that the generation interval does not significantly differ among variants [46–48].

Table 1 discusses the parameters we use and how they differ between variants. We extend that discussion here by showing how these parameters translate into dimensions of primary concern. To simplify a visual presentation, Figure 3 only shows \mathcal{R}_0^V and vaccine effectiveness, which are the two most important measures that are independent of population composition. We further distinguish vaccine effectiveness between mRNA (\circ) and vector (Δ) vaccines. Both estimates and their uncertainty are summarized in Figure 3, in which the parameters are drawn from a truncated normal distribution with mean and truncation points given in Table 1. The uncertainty represented in Figure 3 is also included in our simulations.

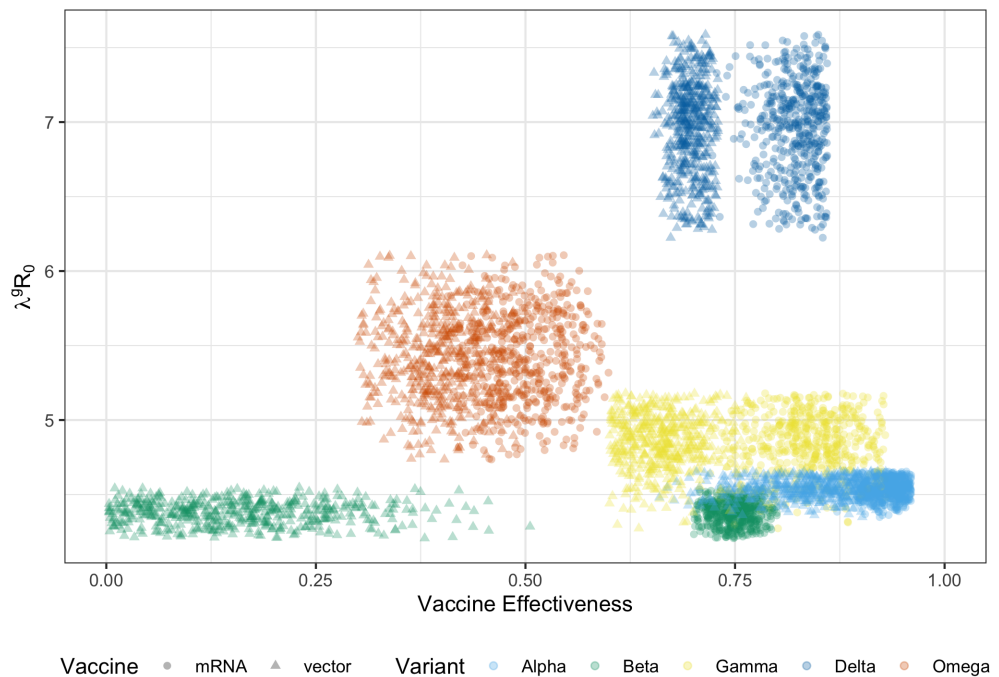


Fig 3. Base reproduction number and vaccine effectiveness against variants we include in our simulations: Alpha (A), Gamma (G), Delta (D), and Omega (O). The Omega variant is constructed to analyze hypothetical scenarios. Note that WT is only present in the history of previous infections.

While Figure 3 summarizes raw parameters, it is not sufficient to characterize which variants are of greater concern within a given population. We also show how these

variant characteristics map to variant risk and are affected by the rise of immune resistance due to vaccinations. These are the two dimensions of primary interest: our risk measure combines both the variant profiles and the background population characteristics, while vaccinations provide the long-term solution to the pandemic. Therefore, our graphs summarize which variants are of greatest concerns to regions with different vaccination rates. $\mathcal{R}_{e,t}^{hg}$ from Equation (4) does not easily allow one to compare variants because it specifies both the group that is being infected as well as depends on mitigation and seasonality. Therefore, we remove time varying components and average over all groups h in the population. Furthermore, in order to discuss a variant V and not merely the infectiousness of a compartment \mathcal{C}^h , this needs to be summed over all compartments with matching final (infectious) character, i.e.,

$$\rho_t^V = N^{-1} \lambda^V \mathcal{R}_0 \sum_{\substack{h \in \mathcal{H} \\ s.t. h = \bar{h}^V}} \sum_{g \in \mathcal{H}} \tilde{\gamma}^{gh} |S_t^g|. \quad (13)$$

This is essentially the base reproduction number of variant V in the current population before mitigation and seasonality.

In order to plot ρ_t^V as a function of the vaccination rate $r \in [0, 1]$, we need to consider how the population composition would change and how this would be reflected in the size of our compartments. As we have created a realistic population distribution for Austria on August 8, 2021, we want to maintain this realism over the range of possible infection rates. Therefore, we split the population into two sets: vaccinated and unvaccinated. The unvaccinated cohort $\mathcal{C}_{uv} = \{\mathcal{C}^h \in \mathcal{C} \text{ s.t. } \mathbb{N} \cap h = \emptyset\}$ and the vaccinated cohort $\mathcal{C}_{va} = \{\mathcal{C}^h \in \mathcal{C} \text{ s.t. } \mathbb{N} \cap h \neq \emptyset\}$. As vaccines are assumed to be given independently of whether or not someone has been previously infected and recovered, this maintains our population distribution. Let \mathcal{H}_{uv} and \mathcal{H}_{va} contain the partitioned histories corresponding to \mathcal{C}_{uv} and \mathcal{C}_{va} , respectively. Lastly, let $N_{va} = \sum_{h \in \mathcal{H}_{va}} |S_t^h|$ and $N_{uv} = \sum_{h \in \mathcal{H}_{uv}} |S_t^h|$ be the size of the vaccinated and unvaccinated susceptible populations, respectively. Note that $N \approx N_{va} + N_{uv}$ as we ignore the comparatively small set of people that are currently infected. We then have

$$\rho_t^V(r) = \lambda^V \mathcal{R}_0 \left(\frac{r}{N_{va}} \sum_{\substack{h \in \mathcal{H}_{va} \\ s.t. h = \bar{h}V}} \sum_{g \in \mathcal{H}} \tilde{\gamma}^{gh} |S_t^g| + \frac{1-r}{N_{uv}} \sum_{\substack{h \in \mathcal{H}_{uv} \\ s.t. h = \bar{h}V}} \sum_{g \in \mathcal{H}} \tilde{\gamma}^{gh} |S_t^g| \right). \quad (14)$$

Observe that Equation (14) is merely a convex combination between ρ_t^V computed on two different populations: those who are vaccinated (first term) and those who are not (second term). For example, suppose that there is no resistance conferred by previous infection and perfect resistance conferred by vaccination ($\tilde{\gamma}^{hV} = 1, \forall h \in \mathcal{H}_{uv}$ and $\tilde{\gamma}^{hV} = 0, \forall h \in \mathcal{H}_{va}$). In this case, Equation (14) simplifies to $\rho_t^V(r) = \lambda^V \mathcal{R}_0(1-r)$, which is just the base reproduction number times the proportion of unvaccinated individuals.

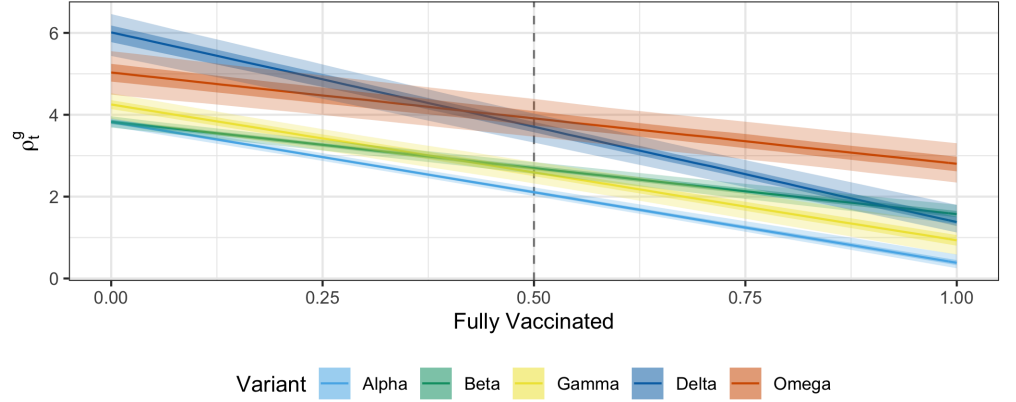


Fig 4. The relative advantage of variants with the composition of the population, namely the extend of immune resistance. A population dependent measure of variant infectiousness, defined in Equation (14), shown as a function of the proportion of population that is vaccinated. The population history reflects Austria on August 8, 2020, with about 20% of population recovered from infections, mainly by WT (75%), Alpha (22%) and Delta (3%). (Note that while Delta is dominant by this time, the absolute number of infections is comparably low). Shaded regions correspond to 50% and 90% prediction intervals resulting from the uncertainty in viral parameters summarised in Figure 3, and the assumed composition of the population is depicted in Figure. For simplicity, we assume that vaccination is independent of the infection history.

Figure 4 shows how $\rho^V(r)$ changes as a function of the proportion of the population that is fully vaccinated, r . In a highly vaccinated population, the Delta and Beta variants are estimated to be similarly infectious, but they diverge significantly in

populations with a lower percentage vaccinated. The bands in Figure 4 capture the uncertainty in parameter values shown in Figure 3. The ranking of risks only switches in the case when a large proportion of the population is vaccinated (thus increasing the average resistance against variants, which were highly transmissible in a more naïve population). This area is unlikely to be reached without wide-spread and thorough vaccination campaigns. For example, only 88% of the Austrian population is in the 12+ age category, and nearly all of this category would need to be vaccinated to reach the change point.

In order to understand what a future outbreak could look like, we hypothesize a new variant, Omega, with lower base effective reproduction number than the currently dominant Delta variant but also lower vaccine effectiveness. This configuration was chosen in order to create a realistic problem setting that can continually affect regions even after successful vaccination campaigns.

Control Types

One long-standing question has been how best to control COVID-19 outbreaks when they arise. This subsection explores which statistics should be considered when determining whether to increase or decrease mitigation measures, particularly after the introduction of a new SARS-CoV-2 variant with higher effective reproduction number. Two control regimes are considered that either respond to increases in case numbers (“reactive” control) or to increases in an estimate of the reproduction number (“proactive” control). We find that using an estimate of the effective reproduction number in addition to case numbers is a more efficient strategy.

Responding to the effective reproduction number further helps to address a potential endogeneity effect due to increasing prevalence of COVID-19, i.e., individuals may modify their behavior when the situation either worsens or improves. Most public reporting discusses solely case numbers, so it may be reasonable to assume that individuals base decisions more on either absolute case levels or strong increases in cases. This can be problematic at the start of a wave if case numbers are incredibly low: purely measuring absolute increases or case-number thresholds may trigger a response too slowly. On the other hand, as the reproduction number is not given the same

attention in the media, individuals may not change behavior dramatically when it changes. This helps connect NPIs to simulation dynamics, as individuals are not also responding to the same statistics as our NPIs.

As mentioned above, we consider two specific control settings. The first, termed “reactive”, only responds to case numbers. There is an upper bound, above which stricter NPIs are used, and a lower bound, below which NPIs are relaxed. This is crafted to mimic the EU protocols for measuring the riskiness of non-essential travel, which assign color codes to regions depending on their publicly reported epidemiological data such as 14-day rate of cases, deaths, and/or tests administered [4]. Being below the lower boundary corresponds to being “green” whereas above the upper corresponds to being “red”. In our results, we show a reactive controller with two different sets of thresholds. The first set, referred to as “low-positivity”, uses a lower bound of 25 cases per 100,000 and an upper bound of 150 cases per 100,000 (both measured over a 14-day period). This corresponds the recommendations for a low test-positivity region. The second set, referred to as “high-positivity”, uses also a lower bound of 25 cases per 100,000 but an upper bound of 50 cases per 100,000 (both measured over a 14-day period). This is far stricter and corresponds to recommendations for a high test-positivity region.

The second control, termed “proactive”, responds to both case numbers and the effective reproduction number $\hat{\mathcal{R}}_{e,t}$ in Equation (12). The same thresholds for case numbers are used as by the reactive control. There is also an upper threshold of 1.2 for $\hat{\mathcal{R}}_{e,t}$. The decision rule is as follows: If $\hat{\mathcal{R}}_{e,t}$ is above its upper threshold or the cases are above the upper threshold whilst $\hat{\mathcal{R}}_{e,t} > 1$, increase restrictions. Conversely, if both $\hat{\mathcal{R}}_{e,t} < 1$ and cases are below their lower threshold, reduce restrictions. In all other cases, make no changes. For both controllers, when mitigation is modified, it is assumed that a 20% change in mitigation is made (both when strengthening and relaxing NPIs).

Delta

We simulate two main scenarios corresponding to both the growth of a new dominant variant and projections for infections after the variant permeates the population. For concreteness and validation in this section, the new variant is the Delta variant. We simulate infection trajectories using initial conditions when Delta accounts for 20% of current infections. For the majority of the world, 20% is no longer an accurate

description of the current state of the pandemic, but this simulation provides two benefits: first, it provides valuable model validation by starting the simulation when 20% *was* accurate for Austria and comparing simulations to observed cases and statistics; second, it furnishes a sample case for what can happen when a new variant with similar transmissibility advantage reaches this threshold.

Our 20% Delta simulation begins on June 12, 2021, as that matches the AGES estimates for Delta prevalence in Austria. The same initialization process was used as discussed previously, merely until June 12 instead of August 8. All other parameters needed to initialize our simulations are also taken from observed data on this day. This includes history of new cases, the proportion of population that is vaccinated or previously infected, etc. Figure 5 shows that our model accurately forecasts the proportion of Delta cases as measured by AGES: this holds true regardless of whether a proactive or reactive control is used, as seen in the bottom panel Figure 6. The result is independent of the controller as the controller affects all variants equally.

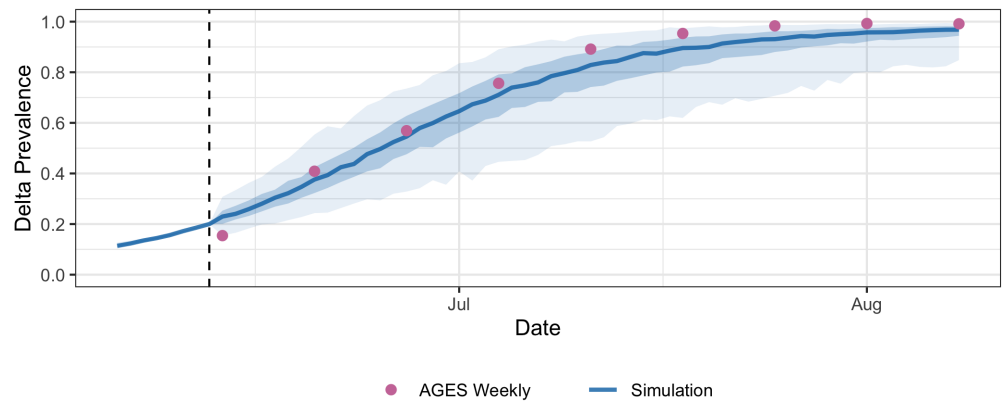


Fig 5. The changing proportion of new Delta cases is accurately predicted. The simulation is initialized using information available on June 12, when the observed proportion of Delta in Austria is 20%.

Simulation results for the low-positivity thresholds are shown in Figure 6, which shows daily incidences (case numbers), the effective mitigation level \tilde{M}_t (reduction in $\mathcal{R}_{e,t}$ due to NPIs), and the current estimate of the effective reproduction number $\hat{\mathcal{R}}_{e,t}$. These additional graphs can be used to more precisely monitor both the simulated COVID-19 epidemic as well as the control process. The first observation from Figure 6

is that the reactive control fits the observed cases over the summer months extremely well. We note that the only real data used beyond the June 12 start date is the vaccination schedule.

Both controllers relax restrictions at roughly the same point (early July), which approximately coincides with the start of the Green Pass program for European tourism on July 1. Approximately one month later, however, the proactive control would increase mitigation measures again to prevent the start of a new outbreak. As case numbers were so low during June, merely looking at new cases yields no increase in NPIs for some time. Alternatively, increasing mitigation earlier stabilizes both the effective reproduction number as well as the the number of new cases.

While the reactive controller in Figure 6 yields case numbers that mimic the observed values very closely, we note that it is not guaranteed in any way that cases will evolve like this in the future. Importantly, the controller begins intervening in the process in early September. If Austria delays in making such changes, it is unlikely that the case numbers will be reduced as shown in our figures.

Figure 7 presents results for the same simulation setting except with the high-positivity case number thresholds. It is clear that simulated cases are much lower as NPIs are triggered more quickly for both controllers due to a stricter upper bound. Case numbers under a reactive controller exhibit a “yo-yo” effect, in which they relatively rapidly cycle through periods of increase and decrease. This effect can also be seen for the low-positivity thresholds of Figure 6, but the timescale is much longer. In general, large peaks lead to sufficiently strict NPIs that subsequent peaks appear much later in our simulations. The proactive controller is much more efficient, and eliminates this behavior almost entirely. Most importantly, however, is that the proactive controller achieved similar control with the low-positivity thresholds. In particular, the left column of Figure 6 shows on average *less strict* NPIs than Figure 7. While case numbers are somewhat higher with higher thresholds, they are still at easily manageable levels for the Austrian medical system.

From the point of view of feasibility, the proactive controller makes far fewer interventions than the reactive controller. While a strict reactive controller does keep case numbers low, this results in interventions which occur almost every two weeks. This is the minimum period that we specify in our model as a gap between interventions.

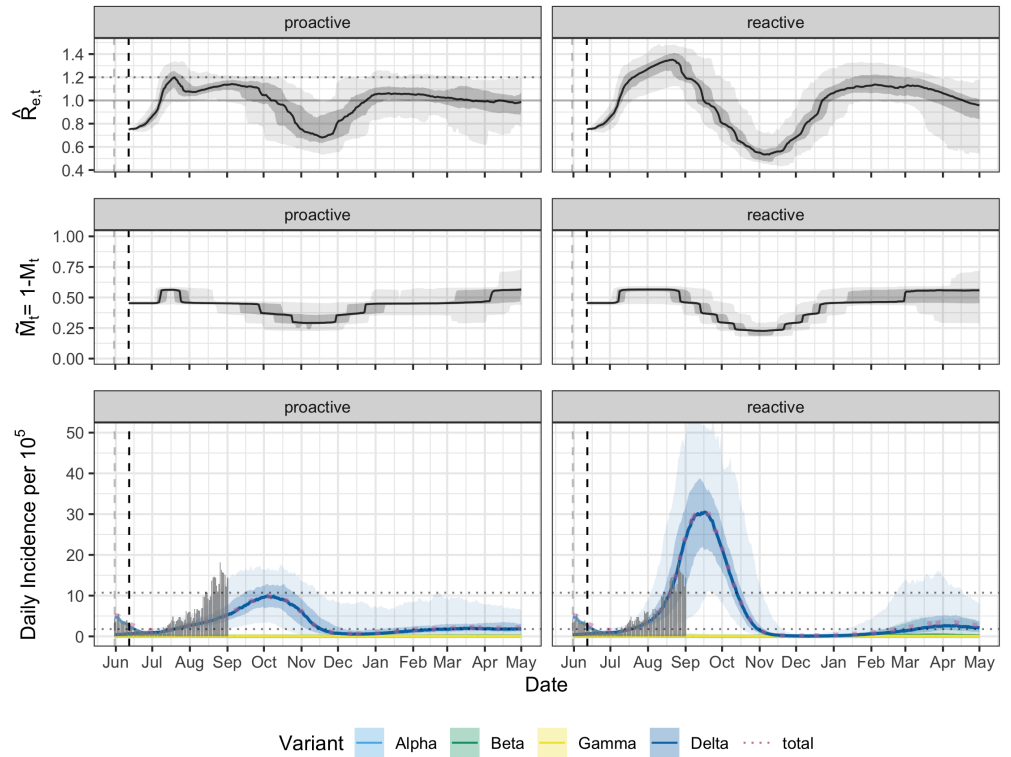


Fig 6. Responding to both the effective reproduction number $\hat{R}_{e,t}$ and the case numbers (proactive control, left) is more efficient than only using the case numbers (reactive control, right). The top row shows the effective reproduction number, middle row the effect of interventions on $\hat{R}_{e,t}$ (where $\tilde{M}_t = 1$ means no NPIs), and bottom row the daily incidence per 100,000 inhabitants. The simulation starts on June 12 (black dashed vertical line) when Delta prevalence was at 20%, and Alpha was the dominant variant. Initializing the model requires use case numbers from the previous 13 days (gray dashed vertical line). The thresholds are shown as dotted horizontal lines and coincide with the WHO recommendations for change in NPIs when positivity rate is low [3, 4]; note that the thresholds, 25 resp. 150 per 100,000 within 14 days are divided by 14 as the y-axis shows daily incidence. The shaded region gives the 50% (dark) resp. 95% (light) confidence interval. The actual incidence in Austria is shown as gray bars, and is matched well by the reactive control with these thresholds.

It is unlikely that a government would be able to so regularly change policy.

New variant

This section introduces a new hypothetical SARS-CoV-2 variant that occupies both a reasonable and empty region of the infectiousness graph in Figure 4. The hypothetical variant, termed Omega, has a lower base reproduction number than Delta but evades immunity after vaccination or infection by older variants more easily. This provides a

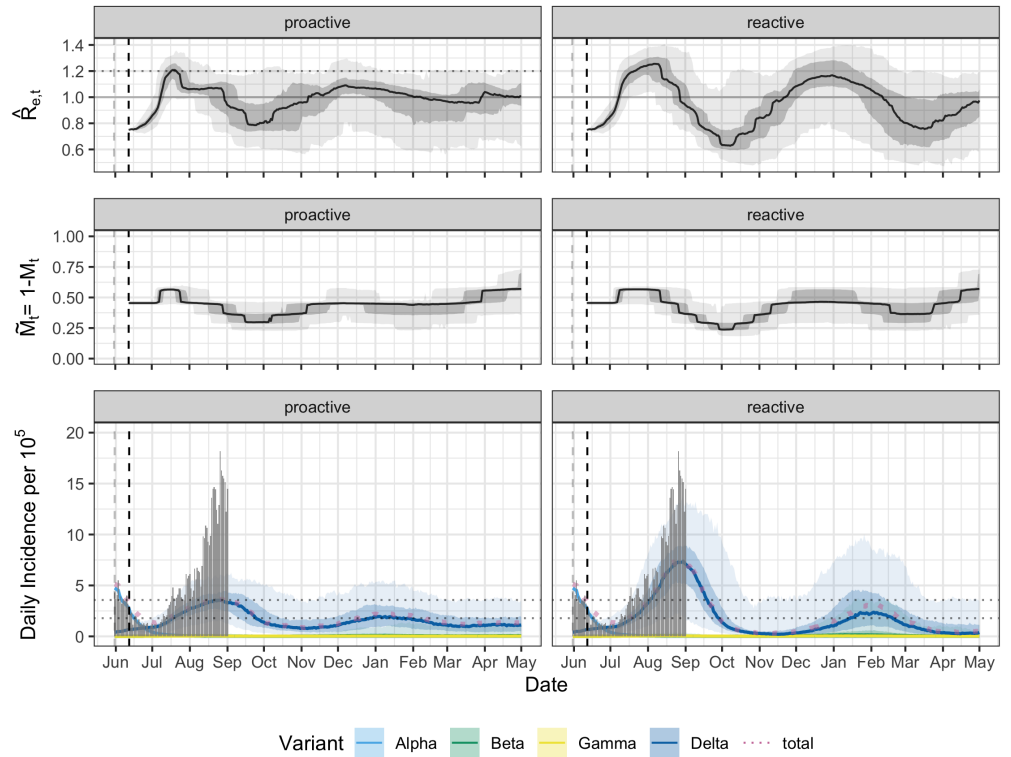


Fig 7. The proactive control is more efficient than reactive control even when incidence thresholds are stricter. Assuming stricter control, where NPIs are increased already when the incidence is 50 per 100,000 inhabitants over a 14 day period, the yoyo effect is effectively prevented with proactive control - but not with reactive control. All other parameters are as in Fig. 6.

scenario in which even a relatively highly vaccinated community will still experience an outbreak and the possibility to explore policies used during the winter of 2021 and spring 2022. Omega is introduced as a weekly import, and for simplicity, one case is imported per day. The distribution of imported cases has no effect on the results, regardless if cases are imported daily or staggered throughout the week. The results are fairly robust to the rate of import of Omega. For example, doubling the import rate primarily reduces the time required to see an outbreak and causes faster yoyo effects for the reactive control (Fig. S1). All other parameter and control settings are the same as in the previous subsection on Delta.

Figure 8 shows how the controls manage the new Omega variant using the low-positivity thresholds (25 and 150 cases/100,000 over 14 days). The first few months of each image look the same as those in Figure 6: the increased mitigation in the fall

delays Omega from being established. The second simulated wave, however, is driven by Omega given the high proportion vaccinated. Given the population vaccination levels and compartment structure in Austria, Omega out-competes Delta when the proportion of vaccinated individuals exceeds 40%, which happened in Austria at the end of May, 2021. The largest difference between scenarios with and without Omega is the width of the intervals for the reactive control. Not only does the reactive control allow larger outbreaks, but it is unable to guarantee that all simulation paths are controlled. In approximately 2.5% of simulations, infections peaked at nearly 35 cases/100,000. The proactive control was able to provide much stronger control on all simulation instances. Furthermore, near the end of the series we see that the reactive controller has actually used more NPIs than the proactive controller.

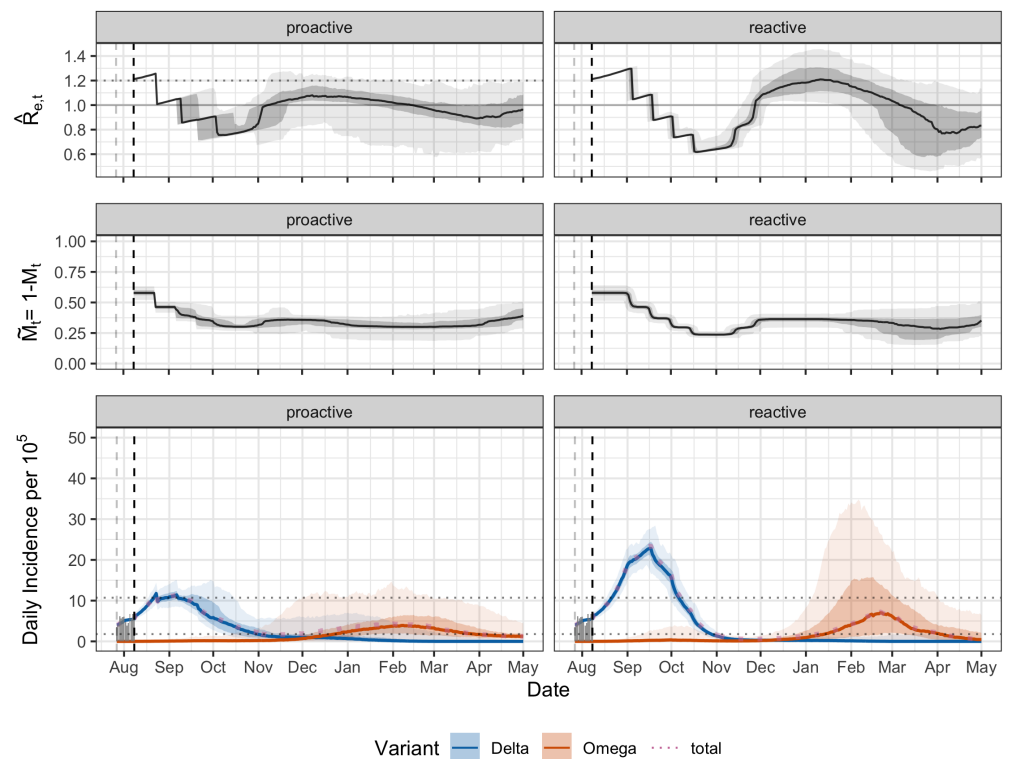


Fig 8. The reactive control fails to contain new variants that are competitive in highly-vaccinated populations. The figure shows a scenario with a hypothetical variant Omega, with lower base reproduction number \mathcal{R}_0 than the Delta variant, but with a higher ability to escape immunity post vaccination or infection by other variants (c.f. Fig. 4). Proactive control prevents an outbreak and uses less NPIs overall. Other parameters are the same as in Fig. 6

As vaccinations increase, some governments may react to hospitalised (or

ICU-hospitalised) incidence instead of case numbers. The rationale is that the controller decides based on hospital capacity, rather than managing the cases. This is particularly enticing as the vaccines reduce severe illnesses or hospitalizations even more than mere infections. Yet, this results in a larger delay in control as there is a larger delay between infection and hospitalization. While we do not model hospitalizations, we can increase the delay that the government suffers for observing cases. This isolates the effect of the delayed information. If hospitalizations are a constant multiple of infections, then our results translate directly to that domain as well.

Figure 9 shows simulation results with the hypothetical Omega variant, using low-positivity WHO thresholds (25 and 150 cases/100,000/14 days), but with a delay of 21 days (instead of 7 days). In this case, the controller is using the same decision rules to increase or decrease NPIs, but the case data informing this decision is 21 days old. This corresponds to the approximate 2-3 week delay between infection and hospitalization at ICU [49]. We see that the initial outbreaks are significantly more pronounced (c.f. Fig. 8), especially for the reactive control. Delayed information cuts both ways, however, as restrictions are increased and maintained far longer than necessary: decreases in transmissions are also not observed quickly. By driving cases down near 0, future waves are delayed. In some simulation paths, Omega outbreaks are observed under reactive control starting in April. In reality, we expect a government to relax sooner, but at the cost of future waves also arriving sooner.

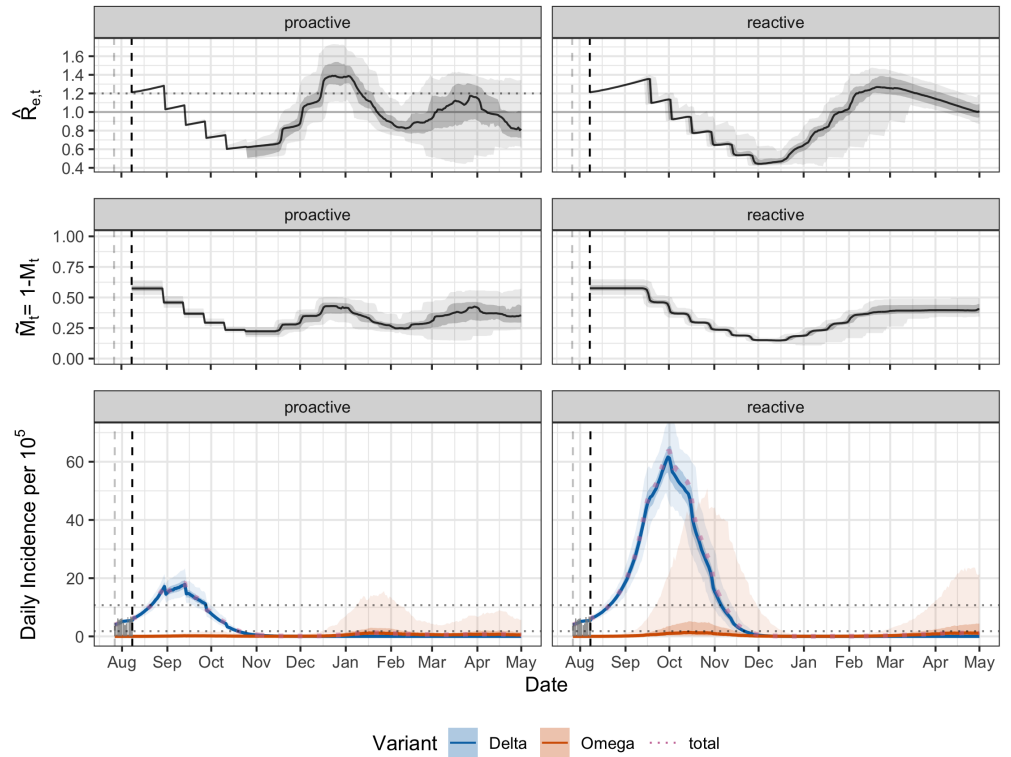


Fig 9. Controller with a larger delay leads to significantly more pronounced outbreaks, especially with reactive control. The figure shows a controller with a 3-week delay. A similar delay would be expected when decisions are based on hospitalizations due to COVID-19, rather than on cases. We (conservatively) assume the thresholds would stay the same. C.f. Fig. 8, where the controller responds with a 1-week delay.

Discussion

The model and simulation that we develop provides significant insight into efficient control strategies of COVID-19 outbreaks. The key behavior which we wanted to capture in our simulation was a complex interaction between diverse groups in a compartment model. Our simulation creates compartments for various vaccines, multiple SARS-CoV-2 variants, and specifies well-supported parameters for them all. The interaction rules between compartments are transparent. This allows us to simulate complex scenarios in a realistic and dynamic setting. Our results show many benefits of looking at the effective reproduction number in addition to case numbers.

A potential limitation of our simulation is our lack of observation level model which would allow us to simulate a fluctuating positivity rate. While some view this to be an

important statistic, we do consider a range of case-based thresholds which span the gamut of positivity rate scenarios. In all of these settings, we find consistent support for using a proactive control strategy that responds to changes in the effective reproduction number.

Our model does not explicitly incorporate any network structure for individuals' interactions; each individual in the simulation interacts independently with all other members. In reality, infections take place in the household, work, and social environments. The different cross-contamination rates in these environments lead to clusters of observed infections, not only in terms of infections occurring, but also in terms of identifying them via contact tracing. This is partially alleviated by our model accounting for super-spreading. Large super-spreading events are often caused by high infectiousness coupled with a particular network structure. By incorporating super-spreading natively in our model, we are able to produce cluster-like effects due to people that are significantly more contagious than others. Furthermore, other changes in network structure are captured by seasonality or mitigation; seasonality can be caused by increased indoor interaction during winter months, and social distancing rules are common NPIs.

Of great concern currently is the effect of waning immunity granted by vaccines. While this is not implemented in our simulation, we do analyze the mirror problem. Instead of reducing vaccine effectiveness over time, we introduce a hypothetical SARS-CoV-2 variant which has an elevated level of escape of vaccination-induced immunity. The resulting effect is a reduced average vaccine efficacy – thus to some extent, the results we present extend to models with waning immunity.

As our model contains many parameters governing diverse characteristics such as vaccine effectiveness, resistance to reinfection (including cross-infection by other variants) and basic reproduction numbers, a natural question is which of these has a stronger effect on the simulation. The difficulty in answering comes down to the distribution of the population across the compartments we describe. Populations with lower vaccination rates but higher rates of previous infection will naturally be more sensitive to cross-infection rates and vice versa. That is why we defined the ρ^V parameter, which characterizes a decisive component of the effective reproduction number. It depends on both \mathcal{R}_0 and the reduction in transmissibility arising from the

(partial) immunity acquired by previous infections and vaccinations within a particular population. We believe ρ^V is an important summary parameter of great relevance.

The paper is not intended to forecast what the future of SARS-CoV-2 will bring: potentially vaccine resistant variants, or variants with even higher base reproduction number, etc. The next important VOC may well have different characteristics to the hypothesised Omega. It is important to keep in mind though, that same VOCs which appear to be currently out-competed by (say) Delta may have a competitive advantage later, e.g., the recently prominent VOC Mu [50]. The possibility of change in the relative advantage between variants is especially relevant should the newly dominant variant also lead to more severe symptoms. The main claims of this paper, however, hold true for all of these possibilities. Regardless of the process leading to future waves, one certainty is that they will occur. In this eventuality, governments must design methods to identify and react to changes in the pandemic. Our results focus on this common denominator.

Acknowledgements

We would like to thank Astrid Christine Erber, Michal Hledík , Pavel Payne and Claudia Zimmermann for insightful discussions and comments on earlier drafts.

References

1. Brauner JM, Mindermann S, Sharma M, Johnston D, Salvatier J, Gavenčiak T, et al. Inferring the effectiveness of government interventions against COVID-19. *Science*. 2021;371(6531).
2. Sharma M, Mindermann S, Rogers-Smith C, Leech G, Snodin B, Ahuja J, et al. Understanding the effectiveness of government interventions in Europe's second wave of COVID-19. *medRxiv*. 2021;doi:<https://doi.org/10.1101/2021.03.25.21254330>.
3. World Health Organization. Critical preparedness, readiness and response actions for COVID-19: interim guidance, 27 May 2021. World Health Organization; 2021.

4. Council of the European Union. Draft Council Recommendation on a coordinated approach to the restriction of free movement in response to the COVID-19 pandemic; 2020. <https://data.consilium.europa.eu/doc/document/ST-11689-2020-REV-1/en/pdf>.
5. Ahn HS, Silberholz J, Song X, Wu X. Optimal COVID-19 containment strategies: Evidence across multiple mathematical models. Available at SSRN. 2021;doi:<http://dx.doi.org/10.2139/ssrn.3834668>.
6. Shea K, Runge MC, Pannell D, Probert WJM, Li SL, Tildesley M, et al. Harnessing multiple models for outbreak management. *Science*. 2020;368(6491):577–579. doi:10.1126/science.abb9934.
7. Johnson KD, Beiglböck M, Eder M, Grass A, Hermisson J, Pammer G, et al. Disease momentum: Estimating the reproduction number in the presence of superspreading. *Infectious Disease Modelling*. 2021;6:706–728. doi:<https://doi.org/10.1016/j.idm.2021.03.006>.
8. Cori A, Ferguson NM, Fraser C, Cauchemez S. A new framework and software to estimate time-varying reproduction numbers during epidemics. *American journal of epidemiology*. 2013;178(9):1505–1512.
9. Richter L, Schmid D, Chakeri A, Maritschnik S, Pfeiffer S, Stadlober E. Schätzung des seriellen Intervalles von COVID19, Österreich; 2020.
10. Knight J, Mishra S. Estimating effective reproduction number using generation time versus serial interval, with application to covid-19 in the Greater Toronto Area, Canada. *Infectious Disease Modelling*. 2020;5:889 – 896. doi:<https://doi.org/10.1016/j.idm.2020.10.009>.
11. Ganyani T, Kremer C, Chen D, Torneri A, Faes C, Wallinga J, et al. Estimating the generation interval for coronavirus disease (COVID-19) based on symptom onset data, March 2020. *Eurosurveillance*. 2020;25(17):2000257.
12. Endo A, Abbott S, Kucharski A, Funk S. Estimating the overdispersion in COVID-19 transmission using outbreak sizes outside China. *Wellcome Open Research*. 2020;5:67. doi:10.12688/wellcomeopenres.15842.2.

13. Monto AS, DeJonge P, Callear AP, Bazzi LA, Capriola S, Malosh RE, et al. Coronavirus occurrence and transmission over 8 years in the HIVE cohort of households in Michigan. *The Journal of infectious diseases*. 2020;.
14. Moriyama M, Hugentobler WJ, Iwasaki A. Seasonality of respiratory viral infections. *Annual review of virology*. 2020;7.
15. Van Doremalen N, Bushmaker T, Morris DH, Holbrook MG, Gamble A, Williamson BN, et al. Aerosol and surface stability of SARS-CoV-2 as compared with SARS-CoV-1. *New England journal of medicine*. 2020;382(16):1564–1567.
16. Kwon T, Gaudreault NN, Richt JA. Seasonal stability of SARS-CoV-2 in biological fluids. *Pathogens*. 2021;10(5):540.
17. Kronfeld-Schor N, Stevenson T, Nickbakhsh S, Schernhammer E, Dopico X, Dayan T, et al. Drivers of infectious disease seasonality: potential implications for COVID-19. *Journal of Biological Rhythms*. 2021;36(1):35–54.
18. Kissler SM, Tedijanto C, Goldstein E, Grad YH, Lipsitch M. Projecting the transmission dynamics of SARS-CoV-2 through the postpandemic period. *Science*. 2020;368(6493):860–868. doi:10.1126/science.abb5793.
19. Gavenčiak T, Monrad JT, Leech G, Sharma M, Mindermann S, Brauner JM, et al. Seasonal variation in SARS-CoV-2 transmission in temperate climates. *medRxiv*. 2021;doi:10.1101/2021.06.10.21258647.
20. Chia PY, Ong SWX, Chiew CJ, Ang LW, Chavatte JM, Mak TM, et al. Virological and serological kinetics of SARS-CoV-2 Delta variant vaccine-breakthrough infections: a multi-center cohort study. *MedRxiv*. 2021;doi:https://doi.org/10.1101/2021.07.28.21261295.
21. Shamier MC, Tostmann A, Bogers S, De Wilde J, IJpelaar J, van der Kleij WA, et al. Virological characteristics of SARS-CoV-2 vaccine breakthrough infections in health care workers. *medRxiv*. 2021;doi:https://doi.org/10.1101/2021.08.20.21262158.

22. Campbell F, Archer B, Laurenson-Schafer H, Jinnai Y, Konings F, Batra N, et al. Increased transmissibility and global spread of SARS-CoV-2 variants of concern as at June 2021. *Eurosurveillance*. 2021;26(24):2100509.
23. Stefanelli P, Trentini F, Guzzetta G, Marziano V, Mammone A, Poletti P, et al. Co-circulation of SARS-CoV-2 variants B.1.1.7 and P.1. *medRxiv*. 2021;.
24. Faria NR, Mellan TA, Whittaker C, Claro IM, Candido DdS, Mishra S, et al. Genomics and epidemiology of the P.1 SARS-CoV-2 lineage in Manaus, Brazil. *Science*. 2021;372(6544):815–821.
25. CDC. Delta Variant:Infections and Spread; 2021. Available from: <https://www.cdc.gov/coronavirus/2019-ncov/variants/delta-variant.html>.
26. Liu Y, Gayle AA, Wilder-Smith A, Rocklöv J. The reproductive number of COVID-19 is higher compared to SARS coronavirus. *Journal of Travel Medicine*. 2020;27(2):taaa021. doi:10.1093/jtm/taaa021.
27. Park M, Cook AR, Lim JT, Sun Y, Dickens BL. A systematic review of COVID-19 epidemiology based on current evidence. *Journal of clinical medicine*. 2020;9(4):967.
28. Eder M, Hermisson J, Hledik M, Hütter C, Iofinova E, Pisupati R, et al. A COVID-19 compartment model for Austria; 2020. Available from: https://epimath.at/static/EpiMathAustria_SEIR_documentation.pdf.
29. Pouwels KB, Pritchard E, Matthews PC, Stoesser N, Eyre DW, Vihta1 KD, et al. Impact of Delta on viral burden and vaccine effectiveness against new SARS-CoV-2 infections in the UK. *medRxiv*. 2021;doi:<https://doi.org/10.1101/2021.08.18.21262237>.
30. Nasreen S, He S, Chung H, Brown KA, Gubbay JB, Buchan SA, et al. Effectiveness of COVID-19 vaccines against variants of concern in Ontario, Canada. *Medrxiv*. 2021;doi:<https://doi.org/10.1101/2021.06.28.21259420>.
31. Hitchings M, Ranzani OT, Dorion M, D'Agostini TL, de Paula RC, de Paula OFP, et al. Effectiveness of the ChAdOx1 vaccine in the elderly during

- SARS-CoV-2 Gamma variant transmission in Brazil. medRxiv. 2021;doi:<https://doi.org/10.1101/2021.07.19.21260802>.
32. Abu-Raddad LJ, Chemaitelly H, Butt AA. Effectiveness of the BNT162b2 Covid-19 vaccine against the B.1.1.7 and B.1.351 variants. *New England Journal of Medicine*. 2021;385.
 33. Madhi SA, Baillie V, Cutland CL, Voysey M, Koen AL, Fairlie L, et al. Efficacy of the ChAdOx1 nCoV-19 Covid-19 vaccine against the B.1.351 variant. *New England Journal of Medicine*. 2021;384(20):1885–1898.
 34. Polack FP, Thomas SJ, Kitchin N, Absalon J, Gurtman A, Lockhart S, et al. Safety and efficacy of the BNT162b2 mRNA Covid-19 vaccine. *New England Journal of Medicine*. 2020;.
 35. Baden LR, El Sahly HM, Essink B, Kotloff K, Frey S, Novak R, et al. Efficacy and safety of the mRNA-1273 SARS-CoV-2 vaccine. *New England Journal of Medicine*. 2021;384(5):403–416.
 36. Voysey M, Clemens SAC, Madhi SA, Weckx LY, Folegatti PM, Aley PK, et al. Safety and efficacy of the ChAdOx1 nCoV-19 vaccine (AZD1222) against SARS-CoV-2: an interim analysis of four randomised controlled trials in Brazil, South Africa, and the UK. *The Lancet*. 2021;397(10269):99–111.
 37. Planas D, Veyer D, Baidaliuk A, Staropoli I, Guivel-Benhassine F, Rajah MM, et al. Reduced sensitivity of SARS-CoV-2 variant Delta to antibody neutralization. *Nature*. 2021; p. 1–7.
 38. Bates TA, Leier HC, Lyski ZL, McBride SK, Coulter FJ, Weinstein JB, et al. Neutralization of SARS-CoV-2 variants by convalescent and BNT162b2 vaccinated serum. *Nature Communications*. 2021;12(1):1–7.
 39. Saad-Roy CM, Morris SE, Metcalf CJE, Mina MJ, Baker RE, Farrar J, et al. Epidemiological and evolutionary considerations of SARS-CoV-2 vaccine dosing regimes. *Science*. 2021;372(6540):363–370.

40. Pegu A, O'Connell S, Schmidt SD, O'Dell S, Talana CA, Lai L, et al. Durability of mRNA-1273 vaccine-induced antibodies against SARS-CoV-2 variants. *Science*. 2021;373(6561):1372–1377.
41. Agentur für Gesundheit und Ernährungssicherheit GmbH. SARS-CoV-2-Varianten in Österreich; 2021.
<https://www.ages.at/themen/krankheitserreger/coronavirus/sars-cov-2-varianten-in-oesterreich/>.
42. Rippinger C, Bicher M, Urach C, Brunmeir D, Weibrecht N, Zauner G, et al. Evaluation of undetected cases during the COVID-19 epidemic in Austria. *BMC Infectious Diseases*. 2021;21(1):1–11.
43. Statistik Austria. Press-conference 12.396-236/20; 2020. Available from: http://www.statistik.at/web_de/statistiken/menschen_und_gesellschaft/gesundheit/covid19/124959.html.
44. Bicher MR, Rippinger C, Schneckenreither GR, Weibrecht N, Urach C, Zechmeister M, et al. Model Based Estimation of the SARS-CoV-2 Immunization Level in Austria and Consequences for Herd Immunity Effects. medRxiv. 2021;doi:<https://doi.org/10.1101/2021.03.10.21253251>.
45. Agentur für Gesundheit und Ernährungssicherheit GmbH. COVID-19 vaccination data for Austria; 2021.
<https://info.gesundheitsministerium.gv.at/data/timeline-eimpfpass.csv>.
46. Blanquart F, Abad C, Ambroise J, Bernard M, Cosentino G, Giannoli JM, et al. Spread of the Delta variant, vaccine effectiveness against PCR-detected infections and within-host viral load dynamics in the community in France; 2021. Available from: <https://hal.archives-ouvertes.fr/hal-03289443/>.
47. Pung R, Mak TM, Kucharski AJ, Lee VJ. Serial intervals in SARS-CoV-2 B.1.617.2 variant cases. *The Lancet*. 2021;398:837–838.
doi:[https://doi.org/10.1016/S0140-6736\(21\)01697-4](https://doi.org/10.1016/S0140-6736(21)01697-4).

48. Hart W, Abbott S, Endo A, Hellewell J, Miller E, Andrews N, et al. Inference of SARS-CoV-2 generation times using UK household data. medRxiv. 2021;doi:<https://doi.org/10.1101/2021.05.27.21257936>.
49. Zhou F, Yu T, Du R, Fan G, Liu Y, Liu Z, et al. Clinical course and risk factors for mortality of adult inpatients with COVID-19 in Wuhan, China: a retrospective cohort study. *The Lancet*. 2020;395(10229):1054–1062.
50. Uriu K, Kimura I, Shirakawa K, Takaori-Kondo A, Nakada Ta, Kaneda A, et al. Ineffective neutralization of the SARS-CoV-2 Mu variant by convalescent and vaccine sera. bioRxiv. 2021;doi:<https://doi.org/10.1101/2021.09.06.459005>.
51. Rippinger C, Bicher M, Urach C, Brunmeir D, Weibrecht N, Zauner G, et al. Evaluation of undetected cases during the COVID-19 epidemic in Austria. *BMC Infectious Diseases*. 2021;doi:10.1186/s12879-020-05737-6.
52. Abbott S, Hellewell J, Thompson RN, Sherratt K, Gibbs HP, Bosse NI, et al. Estimating the time-varying reproduction number of SARS-CoV-2 using national and subnational case counts. *Wellcome Open Research*. 2020;5(112):112.

Supplementary information

Sampling in Practice

We use the following data and parameters specific to Austria

- As generation interval (ω_t) we will choose a discretization of a Gamma-distribution with mean $\mathbb{E} = 4.46$ and standard deviation $s = 2.63$ cut off after day 13 as found by AGES in [9]. We use this generation interval for *all* variants.
- The Austrian population is given by $N = 8.902.600$ (as of 2020-01-01, source: http://www.statistik.at/web_de/presse/122588.html).
- We use the data on the progress of the Austrian vaccination program provided by <https://info.gesundheitsministerium.at/>. Individuals vaccinated with an mRNA respective vector vaccine will be added to the appropriate group 14 respective 21 days after the first dose. We take the median doses of the last 7 days of available data for projecting daily administered doses into the future.
- We use reported incidence provided by <https://covid19.who.int/>. We assume all infections that happened in 2020 were with the wild type and we split the incidence of 2021 according to the AGES data that is given in Figure 1. Furthermore we scale this reported incidence to account for undetected infections based on values found in [51].
- We estimate the observed reproduction number using the R package EpiNow developed in [52].

The sampling procedure is as follows:

- (1) Import data and choose the parameters as above.
- (2) Simulate the overlap between vaccinated and previously infected individuals to determine the group sizes S_t^h .
- (3) Choose initial incidence values, separated into the different variants (e.g. taking constant percentages or fitting a simple model like an exponential growth model) as well as imported cases.

- (4) Let t_0 the the the last day of observed data and let \bar{R}_e denote the effective reproduction number observed on this day. For initializing the model we compute the initial mitigation \tilde{M}_{t_0} using Equation 12 in the following way

$$\tilde{M}_{t_0} = \bar{R}_e W L_{t_0} N \left(\sum_{g \in \mathcal{H}} \sum_{h \in \mathcal{H}} \tilde{\gamma}^{hg} |S_{t_0}^h| \sum_{m=1}^{\nu} \lambda^g \mathcal{R}_0 I_{t_0-m}^g w_m \right)^{-1} .$$

- (5) Sample the model as described in the Methods section.

Supplemental Figures

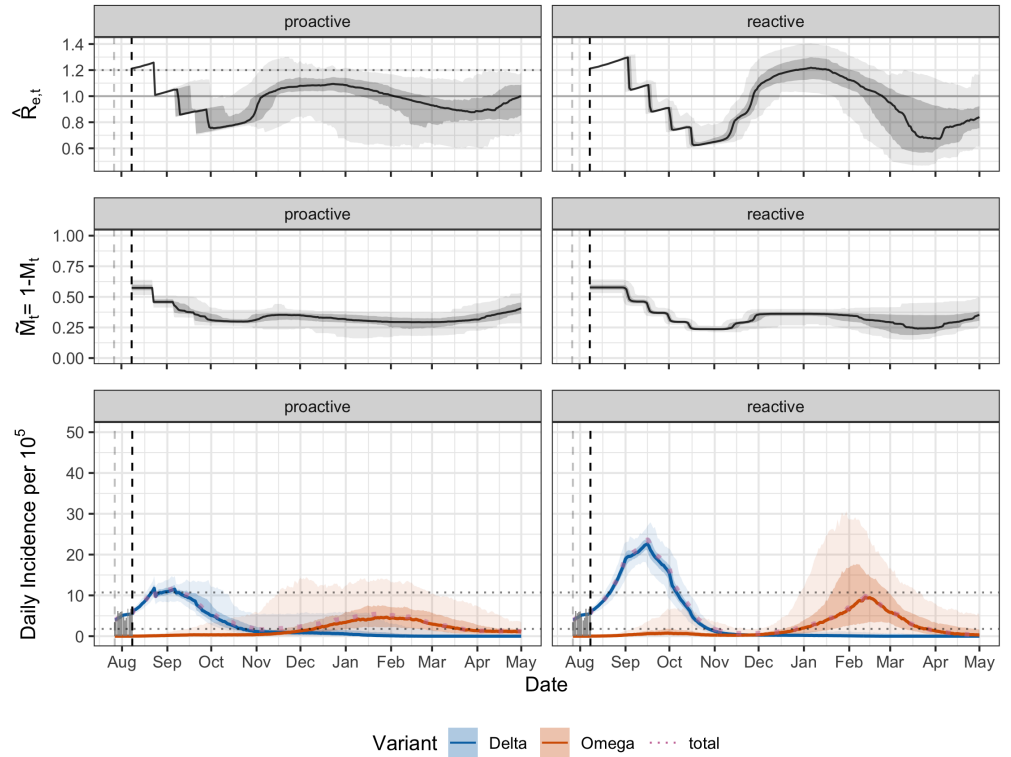


Fig S1. The projected dynamics of the new variant stays similar when the import rate doubles. With double the import rate, the outbreak of Omega merely speeds up slightly. Parameters as in Figure 8 except that we import 2 cases of Omega per day.